Journal of Organometallic Chemistry 695 (2010) 2703–2712

Contents lists available at ScienceDirect

Journal of Organometallic Chemistry

journal homepage: www.elsevier.com/locate/jorganchem

Trivalent lanthanide–alkene complexes: Crystallographic and NMR evidence for coordination of tethered alkenes in the solid state and solution

David J. Berg [a,*], Tosha Barclay [b], Xuening Fei [c]

[a] Department of Chemistry, University of Victoria, P.O. Box 3065 STN CSC, Victoria, B.C., Canada V8W 3V6
[b] Lone Star College – North Harris, Houston, TX 77073-3499, USA
[c] Department of Material Science and Engineering, Tianjin Institute of Urban Construction, Tianjin 300384, PR China

ARTICLE INFO

Article history:
Received 7 July 2010
Received in revised form
23 August 2010
Accepted 1 September 2010
Available online 15 September 2010

This paper is dedicated to the memory of Professor Herbert Schumann: a true pioneer of f-element chemistry, an inspired teacher, an esteemed mentor and above all, a great gentleman.

Keywords:
Lanthanide
f-element
Alkene complex
NMR
Crystallography
X-ray

ABSTRACT

The reaction of 2,6-diallyl-4-methylphenol (H-DALP) and 2-allyl-4,6-dimethylphenol (H-MALP) with Ln[N(SiMe$_3$)$_2$]$_3$ affords dimeric {Ln[DALP]$_2$}$_2$[μ-DALP]$_2$ [Ln = La (**3**), Ce (**4**), Nd (**5**), Er (**6**), Yb (**7**), Y (**8**)] and {Ln[MALP]$_2$}$_2$[μ-MALP]$_2$ [Ln = La (**9**), Sm (**10**), Y (**11**)] complexes, respectively. The solid state structures of **5**, **6**, **8**, **10** and **11** reveal the presence of two weak Ln–alkene interactions per lanthanide center involving one *o*-allyl unit of each terminal aryloxide ligand. Variable temperature NMR studies reveal that the dimeric structures remain intact in non-coordinating solvents with rapid bridge–terminal aryloxide exchange taking place above about 275–295 K for all DALP complexes except erbium. In the case of yttrium complex **8**, evidence for a second dynamic process involving alkene exchange is observed at temperatures below about 220 K. ^{13}C NMR chemical shift data also supports a weak Ln–alkene interaction, although the magnitude of these shifts is small due to rapid averaging of free and bound alkene resonances at higher temperatures. For all complexes, the addition of THF cleaves the dimeric structure and disrupts the Ln–alkene bond.

1. Introduction

Lanthanide–alkene complexes are assumed to be intermediates in a number of catalytic processes mediated by these metals including olefin [1–3] and diene [3–6] polymerization, hydrogenation [3], hydroamination [3, 7–10], hydrophosphination [1, 3] and hydrosilation [1, 3]. Despite their importance, very few lanthanide–alkene complexes have been structurally characterized even though there is ample evidence for their existence from previous NMR studies. Marks showed convincing paramagnetic shift evidence for ethylene coordination to base-free (C$_5$Me$_5$)$_2$Eu [11], and Casey reported extensively on the dynamic NMR behavior of a yttrium alkyl-tethered alkene system of general type (C$_5$Me$_5$)$_2$Y(η^1:η^5-CH$_2$CH$_2$CR$_2$CR′=CH$_2$) (R = H, Me; R′ = H, Me) [12–20]. The latter studies placed the upper limit of ΔG‡ for alkene dissociation at *ca.* 40 kJ mol^{-1} indicating a weak lanthanide–alkene interaction, as might be expected in the absence of any π-backdonation [13,14].

Given that the lanthanide–alkene bond is expected to be weak and labile, it is not surprising that all structurally characterized lanthanide–alkene complexes, with one exception, involve an alkene that is tethered to another coordinating group. The one exception is not a simple alkene at all but rather the Pt-coordinated alkene complex of divalent ytterbium, (C$_5$Me$_5$)$_2$Yb(μ-η^2:η^2-C$_2$H$_4$)Pt(PPh$_3$)$_2$, reported by Andersen and Burns over 20 years ago [21]. This was the first lanthanide–alkene structure reported and remains the only structurally characterized example without alkene tethering. Evans et al. [22] and Schumann et al. [23,24] reported the structures of several alkene-tethered cyclopentadienyl complexes of divalent lanthanides (**I**, **II**, Chart 1) and the closely related alkaline earths (**III**, Chart 1) that show alkene coordination. In fact, other than the interesting alkyl–alkene complex [Yb{η^1:η^2-C(SiMe$_3$)$_2$SiMe$_2$CH=CH$_2$}{OEt$_2$}]$_2$(μ-I)$_2$, (**IV**),

* Corresponding author. Tel.: +1 250 721 7161; fax: +1 250 721 7147.
E-mail address: djberg@uvic.ca (D.J. Berg).

0022-328X/$ – see front matter © 2010 Elsevier B.V. All rights reserved.
doi:10.1016/j.jorganchem.2010.09.004

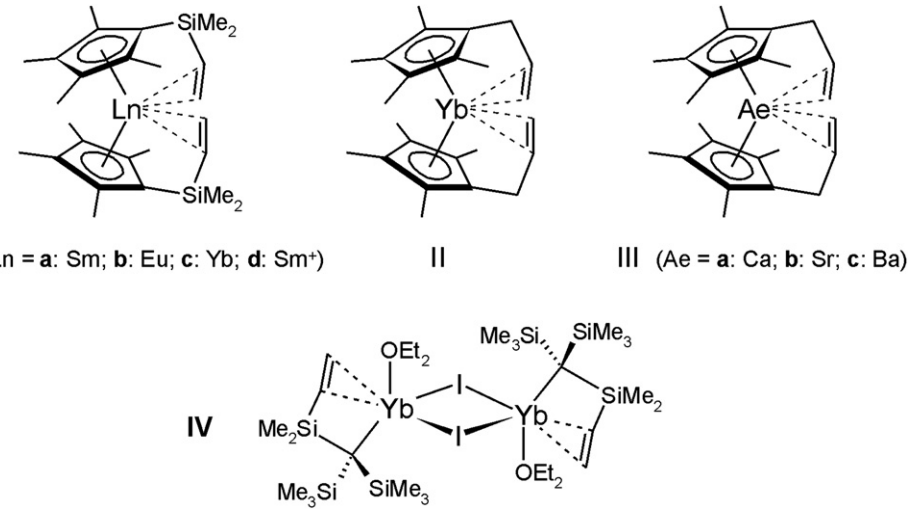

Chart 1.

these represented the extent of structurally characterized lanthanide–alkene complexes prior to this work [25].

In this contribution, we discuss the synthesis, solid state structural features and solution behavior of dimeric lanthanide aryloxides bearing one or two allyl groups in the *o*-aryl positions. Alkene coordination to the Ln^{3+} center from one allyl group of each terminal aryloxide is observed crystallographically across the lanthanide series. These complexes represent the first neutral, trivalent lanthanide–alkene complexes that have been structurally characterized and NMR evidence suggests that the structures obtained in the solid state are maintained in non-coordinating solvents.

2. Experimental

2.1. General procedures

All manipulations were carried out under an argon atmosphere, with the rigorous exclusion of oxygen and water, using standard glovebox (Braun MB150-GII) or Schlenk techniques. Tetrahydrofuran (THF), hexane and toluene were dried by distillation from sodium benzophenone ketyl under argon immediately prior to use. The appropriate lanthanide tris(silylamides), $Ln[N(SiMe_3)_2]_3$, was prepared according to a literature procedure [26].

All NMR spectra (^1H, 360 MHz; ^{13}C, 90 MHz) including variable temperature experiments were recorded on a Bruker AMX-360 MHz spectrometer and referenced to residual solvent resonances. Deuterated solvents were dried over activated 4 Å molecular sieves and spectra were recorded using 5 mm tubes fitted with a Teflon™ valve (Brunfeldt). NMR data for diamagnetic complexes are given at ambient temperature unless otherwise specified; data for paramagnetic complexes are given at selected temperatures. In the ^{13}C DEPT-135 spectra, resonance phases are indicated by + or − in the data below. Complete variable temperature NMR data for the paramagnetic DALP complexes **4**–**7** including plots of δ vs. $1/T$, complete listings of chemical shifts and peak widths at half height are given in the Supplementary Material. Melting points were recorded using a Büchi melting point apparatus and are not corrected. Elemental analyses were performed by Canadian Microanalytical, Delta, B.C. Mass spectra were recorded on a Kratos Concept H spectrometer using electron impact (70 eV) or FAB methods. Only metal complexes **3**, **5** and **7** gave high mass peaks in the mass spectrum under any of the conditions used.

2.2. Ligand synthesis

2.2.1. 2,6-diallyl-4-methylphenol, H-DALP (*1*)

4-Methylphenol (75.6 g, 0.70 mol) was dissolved in 250 mL toluene in a 1 L round bottom flask and 250 mL water was added. Excess NaOH (29 g), tricaprylmethylammonium chloride (12 g) and allyl bromide (93.2 g, 1.1 equiv) were added and the two-phase mixture was heated at 70 °C overnight. After cooling, the organic phase was separated and washed with a further 250 mL water, followed by drying over anhydrous $MgSO_4$. Filtration and removal of the solvent from the filtrate under reduced pressure afforded crude 4-methylphenyl allyl ether (94.3 g, 91%). The allyl ether was then heated as a neat oil at 180 °C for 24 h to afford the Claissen product 2-allyl-4-methylphenol as a light yellow oil in 60% yield (62.2 g) after column chromatography on silica gel (15% ether in hexane). Repeating the above reactions with 2-allyl-4-methylphenol (40 g, 0.27 mol) afforded 32.3 g (64%) of 2,6-diallyl-4-methylphenol, H-DALP (**1**), after chromatography on silica gel (hexane eluent). ^1H NMR (C_6D_6) δ 6.73 (s, 2H, aryl*H*), 5.90 (m, 2H, C*H*=), 5.01 (d, 2H, trans- =C*H*$_2$), 4.96 (m, 2H, cis- =C*H*$_2$), 4.75 (s, 1H, O*H*), 3.23 (d, 4H, C*H*$_2$), 2.12 (s, 3H, C*H*$_3$); $^{13}C\{^1H\}$ NMR (C_6D_6) δ 150.8 (arylCOH), 137.0 (*C*H=), 129.6 (*p*-aryl*C*), 129.5 (*m*-aryl*C*), 125.7 (*o*-aryl*C*), 116.0 (=*C*H$_2$), 35.4 (*C*H$_2$), 20.6 (*C*H$_3$). High Res. MS (EI) Found (Calcd): M^+ 188.1208 (188.1201).

2.2.2. 2-Allyl-4,6-dimethylphenol, H-MALP (*2*)

2-allyl-4,6-dimethylphenol was prepared from 2,4-dimethylphenol using a procedure analogous to that for **1** above. H-MALP (**2**) was isolated as a yellow oil after chromatography on silica gel (15% ether in hexane). Yield: 53% overall (4.20 g of **2** from 6.1 g starting phenol). ^1H NMR (C_6D_6) δ 6.77 (s, 1H, aryl*H*), 6.70 (s, 1H, aryl*H*), 5.93 (m, 1H, C*H*=), 5.02 (m, 2H, =C*H*$_2$), 4.60 (s, 1H, O*H*), 3.20 (d, 2H, CH$_2$, $^3J_{HH}$ = 6.6 Hz), 2.17 (s, 3H, C*H*$_3$), 2.14 (s, 3H, C*H*$_3$); $^{13}C\{^1H\}$ NMR (C_6D_6) δ 150.3 (arylCOH), 137.0 (*C*H=), 129.9 (arylCH), 129.5 (*p*-aryl*C*), 128.5 (arylCH), 124.4, 124.0 (*o*-aryl*C*), 116.2 (=*C*H$_2$), 35.6 (*C*H$_2$), 20.4 (*C*H$_3$), 15.8 (*C*H$_3$). High Res. MS (EI) Found (Calcd): M^+ 162.1043 (162.1045).

2.3. Complex synthesis

2.3.1. {La[DALP]$_2$}$_2$[μ-DALP]$_2$ (*3*)

A solution of **1** (0.250 g, 1.33 mmol) in 4 mL toluene was added to a solution of $La[N(SiMe_3)_2]_3$ (0.274 g, 0.442 mmol) in 16 mL toluene

in the glovebox. An immediate pale green color developed but the solution soon faded to very pale yellow on stirring at room temperature. After stirring overnight, the solvent was removed under reduced pressure and the pasty solid residue was redissolved in hot hexane, filtered though a Celite pad and the filtrate was allowed to cool slowly to room temperature. The cream colored flaky plates of **3** that deposited from solution were collected by suction filtration and dried under vacuum. Yield: 0.23 g (74%). Mp. 152–154 °C; ^{1}H NMR (C_6D_6) δ 6.86 (s, 12H, aryl*H*), 6.09 (m, 12H, C*H*═), 5.16 (m, 24H, ═C*H*$_2$ overlapping), 3.50 (d, 24H, C*H*$_2$), 2.20 (s, 18H, C*H*$_3$); ^{13}C{^{1}H} NMR (C_6D_6) δ 140.7 (*C*H═), 129.4 (*m*-aryl*C*), 117.0 (═*C*H$_2$), 36.1 (*C*H$_2$), 20.7 (*C*H$_3$); the quaternary aryl carbons were not observed; ^{13}C{^{1}H} NMR (C_6D_6:C_4D_8O, 5:1) δ 160.0 (arylCO), 139.1 (*C*H═), 127.0 (*m*-aryl*C*), 115.0 (═*C*H$_2$), 35.5 (*C*H$_2$), 20.8 (*C*H$_3$); the remaining quaternary aryl carbons were not observed; MS (EI) *m*/*z* 1214 ([La$_2$(DALP)$_5^{\ddagger}$] + 1) amu; Anal. Calcd for $C_{78}H_{90}O_6La_2$: C, 66.85; H, 6.47%; Found: C, 66.03; H, 6.63%. The elemental analysis on this compound was repeated several times but this is the best result that was obtained.

2.3.2. {Ce[DALP]$_2$}$_2$[μ-DALP]$_2$ (**4**)

Complex **4** was prepared using a procedure analogous to **3** from Ce[N(SiMe$_3$)$_2$]$_3$ (0.250 g, 0.403 mmol) and 3 equiv of **1**. Deep yellow plates of **4** were isolated from hexane solution. Yield: 0.155 g (55%). Mp. 120–122 °C; ^{1}H NMR (C_7D_8, 297 K) δ 9.22 (24H, C*H*$_2$, $\nu_{1/2}$ = 140 Hz), 2.66 (18H, C*H*$_3$, $\nu_{1/2}$ = 400 Hz), 1.33 (12H, C*H*═, $\nu_{1/2}$ = 160 Hz), −3.29 (12H, C*H*═, $\nu_{1/2}$ = 780 Hz), −7.19 (12H, C*H*═, $\nu_{1/2}$ = 900 Hz), aryl*H* not observed; ^{1}H NMR (C_7D_8, 377 K) δ 6.28 (24H, C*H*$_2$, $\nu_{1/2}$ = 60 Hz), 7.21 (12H, aryl*H*, $\nu_{1/2}$ = 56 Hz), 2.44 (12H, C*H*═, $\nu_{1/2}$ = 48 Hz), 2.35 (18H, C*H*$_3$, $\nu_{1/2}$ = 23 Hz), −0.65 (12H, C*H*═, $\nu_{1/2}$ = 38 Hz), −2.42 (12H, C*H*═, $\nu_{1/2}$ = 40 Hz); Anal. Calcd for $C_{78}H_{90}O_6Ce_2$: C, 66.74; H, 6.46%; Found: C, 66.34; H, 6.71%.

2.3.3. {Nd[DALP]$_2$}$_2$[μ-DALP]$_2$ (**5**)

Complex **5** was prepared using a procedure analogous to **3** from Nd[N(SiMe$_3$)$_2$]$_3$ (0.277 g, 0.443 mmol) and 3 equiv of **1**. Deep blue prisms of **5**, suitable for X-ray crystallography, were isolated from hexane solution. Yield: 0.211 g (68%). Mp. 158–160 °C; MS (EI) *m*/*z* 1226 ([Nd$_2$(DALP)$_5^{\ddagger}$] + 1) amu showing the extensive isotope pattern of Nd; ^{1}H NMR (C_7D_8, 293 K) δ 16.76 (24H, C*H*$_2$, $\nu_{1/2}$ = 500 Hz), 3.7 (18H, C*H*$_3$, $\nu_{1/2}$ = 1300 Hz), −3.46 (12H, C*H*═, $\nu_{1/2}$ = 250 Hz), remaining alkene H and aryl*H* not observed; ^{1}H NMR (C_7D_8, 373 K) δ 10.04 (24H, C*H*$_2$, $\nu_{1/2}$ = 96 Hz), 7.83 (12H, aryl*H*, $\nu_{1/2}$ = 160 Hz), 2.77 (18H, C*H*$_3$, $\nu_{1/2}$ = 64 Hz), 0.18 (12H, C*H*═, $\nu_{1/2}$ = 80 Hz), −3.39 (12H, C*H*═, $\nu_{1/2}$ = 120 Hz), −6.46 (12H, C*H*═, $\nu_{1/2}$ = 145 Hz); Anal. Calcd for $C_{78}H_{90}O_6Nd_2$: C, 66.35; H, 6.42%; Found: C, 65.84; H, 6.15%.

2.3.4. {Er[DALP]$_2$}$_2$[μ-DALP]$_2$ (**6**)

Complex **6** was prepared using a procedure analogous to **3** from Er[N(SiMe$_3$)$_2$]$_3$ (0.287 g, 0.443 mmol) and 3 equiv of **1**. Well-formed, bright pink cubes of **6**, suitable for X-ray crystallography, were isolated from hexane solution. Yield: 0.23 g (71%). Mp. 162–163 °C; ^{1}H NMR (C_7D_8, 298 K) δ 189.4 (16H, $\nu_{1/2}$ = 3500 Hz), 117.3 (8H, $\nu_{1/2}$ = 1000 Hz), 108.6 (8H, $\nu_{1/2}$ = 2300 Hz), 73.3 (8H, $\nu_{1/2}$ = 850 Hz), 45.3 (4H, $\nu_{1/2}$ = 1200 Hz), 8.4 (4H, $\nu_{1/2}$ = 1000 Hz), −11.0 (4H, $\nu_{1/2}$ = 1200 Hz), −28.0 (8H, $\nu_{1/2}$ = 320 Hz), −47.1 (6H, $\nu_{1/2}$ = 400 Hz), −68.1 (12H, $\nu_{1/2}$ = 1200 Hz), −84.6 (8H, $\nu_{1/2}$ > 5000 Hz), one resonance of relative integration 4H was not observed; Anal. Calcd for $C_{78}H_{90}O_6Er_2$: C, 64.25; H, 6.22%; Found: C, 64.17; H, 6.22%.

2.3.5. {Yb[DALP]$_2$}$_2$[μ-DALP]$_2$ (**7**)

Complex **7** was prepared using a procedure analogous to **3** from Yb[N(SiMe$_3$)$_2$]$_3$ (0.290 g, 0.443 mmol) and 3 equiv of **1**. Yellow–orange, flaky plates of **7** deposited from hexane solution. Yield: 0.055 g (17%). Mp. 130–134 °C; MS (EI) *m*/*z* 1469 (M^+ isotopic cluster) amu; ^{1}H NMR (C_7D_8, 297 K) δ 36.07 (12H, C*H*═, $\nu_{1/2}$ = 750 Hz), 25.14 (12H, C*H*═, $\nu_{1/2}$ = 500 Hz), 13.44 (12H, aryl*H*, $\nu_{1/2}$ = 200 Hz), 3.48 (18H, C*H*$_3$, $\nu_{1/2}$ = 15 Hz), −12.46 (24H, C*H*$_2$, $\nu_{1/2}$ = 540 Hz), one alkene H resonance was not observed; ^{1}H NMR (C_7D_8, 377 K) δ 22.95 (12H, C*H*═, $\nu_{1/2}$ = 42 Hz), 17.82 (12H, C*H*═, $\nu_{1/2}$ = 56 Hz), 11.60 (12H, aryl *H*, $\nu_{1/2}$ = 42 Hz), 2.78 (18H, C*H*$_3$, $\nu_{1/2}$ = 5 Hz), −3.99 (24H, C*H*$_2$, $\nu_{1/2}$ = 76 Hz), −19.78 (12H, C*H*═, $\nu_{1/2}$ = 800 Hz); Anal. Calcd for $C_{78}H_{90}O_6Yb_2$: C, 63.75; H, 6.17%; Found: C, 63.24; H, 6.18%.

2.3.6. {Y[DALP]$_2$}$_2$[μ-DALP]$_2$ (**8**)

Complex **8** was prepared using a procedure analogous to **3** from Y[N(SiMe$_3$)$_2$]$_3$ (0.252 g, 0.442 mmol) and 3 equiv of **1**. Colorless cubes of **8** were isolated from hexane solution. Recrystallization from hot a hexane solution afforded crystals suitable for X-ray diffraction. Yield: 0.275 g (95%). Mp. 163–164 °C; ^{1}H NMR (C_6D_6) δ 6.87 (s, 12H, aryl*H*), 5.98 (m, 12H, C*H*═), 5.08 (m, 24H, ═C*H*$_2$ overlapping), 3.50 (d, 24H, C*H*$_2$), 2.15 (s, 18H, C*H*$_3$); ^{1}H NMR (C_6D_6:C_4H_8O, 5:1) δ 6.85 (s, 12H, aryl*H*), 5.97 (m, 12H, C*H*═), 4.92 (m, 24H, ═C*H*$_2$ overlapping), 3.42 (d, 24H, C*H*$_2$), 2.05 (s, 18H, C*H*$_3$); ^{13}C{^{1}H} NMR (C_6D_6) δ 140.1 (very broad, *C*H═), 128.9 (*m*-aryl*C*), 116.5 (very broad, ═*C*H$_2$), 36.7 (*C*H$_2$), 20.8 (*C*H$_3$); the quaternary aryl carbons were not observed; ^{13}C{^{1}H} NMR (C_6D_6:C_4H_8O, 5:1) δ 158.0 (arylCO), 139.1 (*C*H═), 124.7 (*m*-aryl*C*), 114.9 (═*C*H$_2$), 35.2 (*C*H$_2$), 20.9 (*C*H$_3$); the remaining quaternary aryl carbons were not observed; ^{13}C DEPT-135 NMR (C_7D_8, 298 K) δ 139.8 (+, very broad, *C*H═), 128.9 (+, *m*-aryl*C*), 116.7 (−, broad, ═*C*H$_2$), 35.8 (−, *C*H$_2$), 20.7 (+, *C*H$_3$); ^{13}C DEPT-135 NMR (C_7D_8, 203 K) δ 143.3 (+, terminal-OAr *C*H═), 136.4 (+, bridge-OAr *C*H═), 130.2 (+, terminal-OAr *m*-aryl*C*), 128.8 (+, bridge-OAr *m*-aryl*C*), 119.9 (−, bridge-OAr ═*C*H$_2$), 117.6 (−, terminal-OAr ═*C*H$_2$), 37.6 (−, terminal-OAr *C*H$_2$), 35.4 (−, bridge-OAr *C*H$_2$), 27.0 (+, bridge-OAr *C*H$_3$), 21.9 (+, terminal-OAr *C*H$_3$); Anal. Calcd for $C_{78}H_{90}O_6Y_2$: C, 71.99; H, 6.97%; Found: C, 71.55; H, 6.92%.

2.3.7. {La[MALP]$_2$}$_2$[μ-MALP]$_2$ (**9**)

Complex **9** was prepared using a procedure analogous to **3** from La[N(SiMe$_3$)$_2$]$_3$ (0.085 g, 0.14 mmol) and 3 equiv of **2**. Colorless crystals of **9** were isolated from hexane solution. Yield: 0.058 g (67%). Mp. 144–147 °C; ^{1}H NMR (C_6D_6) δ 6.82 (s, 6H, aryl*H*), 6.71 (s, 6H, aryl*H*), 5.89 (m, 6H, C*H*═), 5.02 (d, 6H, *trans*- ═C*H*$_2$), 4.94 (m, 6H, *cis*- ═C*H*$_2$), 3.31 (br m, 12H, CH$_2$), 2.43 (s, 18H, C*H*$_3$), 2.15 (s, 18H, C*H*$_3$); ^{13}C{^{1}H} NMR (C_6D_6) δ 143 (very broad, *C*H═), 130.5 (aryl*C*H), 128.6 (aryl*C*H), 116.5 (broad ═*C*H$_2$), 36.4 (very broad, *C*H$_2$), 20.6 (*C*H$_3$), 17.9 (*C*H$_3$); Anal. Calcd for $C_{66}H_{78}O_6La_2$: C, 63.67; H, 6.31%; Found: C, 64.24; H, 6.78%. This is the best elemental analysis obtained from several trials.

2.3.8. {Sm[MALP]$_2$}$_2$[μ-MALP]$_2$ (**10**)

Complex **10** was prepared using a procedure analogous to **3** from Sm[N(SiMe$_3$)$_2$]$_3$ (0.125 g, 0.200 mmol) and 3 equiv of **2**. Small, colorless crystals of **10** were isolated from hexane solution. Yield: 0.077 g (61%). Mp. 112–116 °C; ^{1}H NMR (C_6D_6) δ 6.45 (br s, 6H, aryl*H*), 6.35 (br s, 6H, aryl*H*), 4.74 (br s, 12H, ═C*H*$_2$), 4.23 (br s, 6H, C*H*═), 3.27 (br s, 18H, C*H*$_3$), 1.81 (br s, 18H, C*H*$_3$); the allyl C*H*$_2$ resonance was not observed but may lay under the 1.81 ppm resonance based on integrated intensities; Anal. Calcd for $C_{66}H_{78}O_6Sm_2$: C, 62.51; H, 6.20%; Found: C, 62.77; H, 6.40%.

2.3.9. {Y[MALP]$_2$}$_2$[μ-MALP]$_2$ (**11**)

Complex **11** was prepared using a procedure analogous to **3** from Y[N(SiMe$_3$)$_2$]$_3$ (0.115 g, 0.200 mmol) and 3 equiv of **2**. Colorless cubes of **11**, suitable for X-ray crystallography, were isolated by repeated crystallization from hexane solution. Yield: 0.038 g (33%). Mp. 167–170 °C; ^{1}H NMR (C_6D_6) δ 6.82 (s, 6H, aryl*H*), 6.71 (s, 6H,

Table 1
Summary of crystallographic data.[a]

	5	6	8	10	11
Formula	$C_{78}H_{90}O_6Nd_2$	$C_{78}H_{90}O_6Er_2$	$C_{78}H_{90}O_6Y_2$	$C_{66}H_{78}O_6Sm_2$	$C_{66}H_{78}O_6Y_2$
fw	1412.1	1458.0	1301.3	1268.0	1145.1
Cryst syst	Monoclinic	Monoclinic	Monoclinic	Triclinic	Triclinic
Space group	$P2_1/n$ (No. 14)	$P2_1/n$ (No. 14)	$P2_1/n$ (No. 14)	$P-1$ (No. 2)	$P-1$ (No. 2)
a (Å)	13.292(3)	13.178(2)	13.183(2)	10.689(3)	10.654(2)
b (Å)	17.272(4)	17.357(3)	17.327(2)	12.237(4)	12.208(2)
c (Å)	16.407(4)	16.233(3)	16.241(2)	12.806(4)	12.803(2)
α (deg)	90	90	90	114.441(5)	115.060(2)
β (deg)	109.006(3)	109.265(3)	109.159(3)	95.824(5)	96.102(3)
γ (deg)	90	90	90	93.432(5)	93.136(3)
V (Å^3)	3561.6(13)	3505.2(10)	3504.3(8)	1507.5(8)	1490.7(4)
Z	2	2	2	1	1
ρ_{calc} (g cm^{-3})	1.32	1.38	1.23	1.40	1.28
μ (mm^{-1})	1.49	2.43	1.70	1.98	1.99
$2\theta_{max}$ (deg)	50	50	50	50	50
meas. refl.	18,483	18,299	18,486	11,228	11,132
unique refl.	6280	6184	6191	5289	5222
refl. $I > 2\sigma(I)$	4727	4241	3177	4953	4255
F_{000}	1452	1484	1368	646	600
R,[b] R_w[c]	0.038, 0.100	0.030, 0.071	0.050, 0.110	0.023, 0.058	0.036, 0.092
R[b] (all data)	0.054	0.059	0.119	0.025	0.049
GOF	1.03	0.92	0.89	1.04	0.98

[a] Collected using a Smart 1000 CCD system (graphite-monochromated Mo K_α $\lambda = 0.71073$ Å at 223 K).
[b] $R = \Sigma(|F_o| - |F_c|)/\Sigma|F_o|$.
[c] $R_w = [\Sigma w(|F_o| - |F_c|^2)/\Sigma w(|F_o|)^2]^{1/2}$.

arylH), 5.89 (m, 6H, CH═), 5.01 (m, 6H, *trans*- ═CH_2), 4.95 (m, 6H, *cis*- ═CH_2), 3.31 (broad m, 12H, CH_2), 2.42 (s, 18H, CH_3), 2.14 (s, 18H, CH_3); $^{13}C\{^1H\}$ NMR (C_6D_6) δ 156.2 (broad, arylCO), 143.4 (broad, CH═), 130.6 (arylCH), 128.7 (arylCH), 126.1 (broad, arylC), 116.5 (broad, ═CH_2), 36.4 (CH_2), 20.7 (CH_3), 18.0 (CH_3); Anal. Calcd for $C_{66}H_{78}O_6Y_2$: C, 69.22; H, 6.87%; Found: C, 68.88; H, 6.73%.

2.4. X-ray crystallographic studies

Crystals suitable for X-ray diffraction were grown from a hot, saturated hexane solution by slow cooling to room temperature in the glovebox. Crystals were mounted on a glass fiber and sealed in epoxy prior to analysis. Data was collected at 223(1) K using a Bruker SMART 1000 instrument (Mo Kα radiation, $\lambda = 0.71073$ Å). Data reduction and correction for Lorentzian polarization and decay were performed using the SHELXTL software [27]. Absorption corrections were applied using SADABS [28]. The structure was solved by direct methods and refined by least squares method on F^2 using SHELXS-97 [29]. All non-hydrogen atoms were refined anisotropically and hydrogen atoms refined isotropically using a riding model. Disorder was observed in some of the non-coordinating allyl groups in each structure. This was modeled using major and minor fragments in approximately 80:20 ratio. Details of the data collection and refinement are given in Table 1.

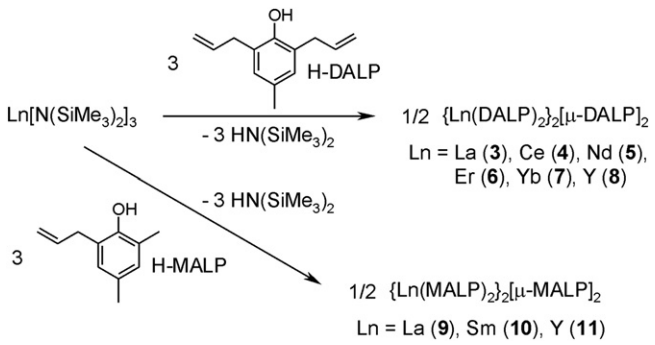

Scheme 1.

3. Results and discussion

3.1. Complex syntheses and solid state structures

Reaction of 3 equivalents of 2,6-diallyl-4-methylphenol (H-DALP) or 2-allyl-4-methylphenol (H-MALP) with Ln[N(SiMe$_3$)$_2$]$_3$ afforded the dimeric tris(phenoxide) complexes {Ln[DALP]$_2$}$_2$[μ-DALP]$_2$ (Ln = La (**3**), Ce (**4**), Nd (**5**), Er (**6**), Yb (**7**), Y (**8**)) or {Ln[MALP]$_2$}$_2$[μ-MALP]$_2$ (Ln = La (**9**), Sm (**10**), Y (**11**)), respectively (Scheme 1). In the case of the colorless complexes of yttrium and lanthanum, initial mixing of the phenol with Ln[N(SiMe$_3$)$_2$]$_3$ resulted in a green colored solution that faded to colorless after

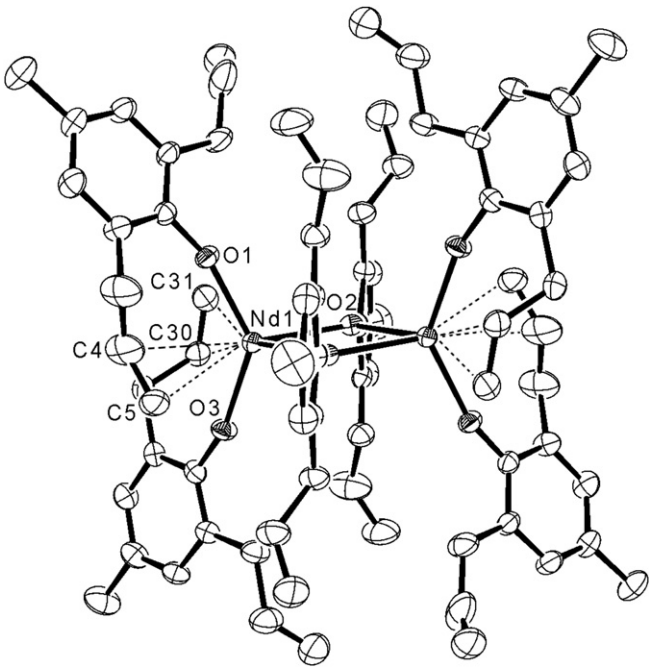

Fig. 1. ORTEP3 plot (30% probability) of {Nd[DALP]$_2$}$_2$[μ-DALP]$_2$ (**5**) [30].

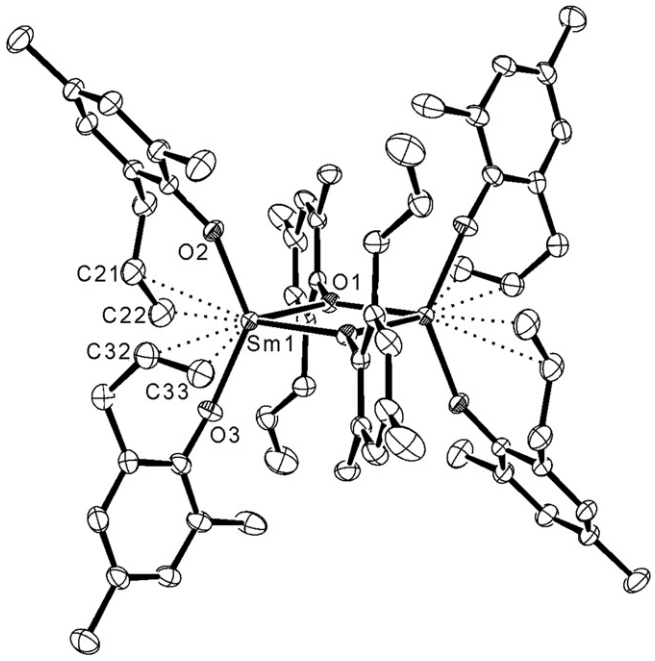

Fig. 2. ORTEP3 plot (30% probability) of {Sm[MALP]$_2$}$_2$[μ-MALP]$_2$ (**10**) [30].

about 15 min, possibly suggesting the formation of transient DALP or MALP phenoxyl radicals [30]. The complexes were recrystallized from hot hexane to afford crystals suitable for X-ray crystallography in most cases. However, crystals of **4** (Ce) and **7** (Yb) were of lower quality. This may indicate the presence of some impurities as these two complexes also gave consistently lower melting points than the rest of the series.

The DALP complexes of Nd (**5**), Er (**6**) and Y (**8**) are isostructural in the monoclinic space group $P2_1/n$; a representative structure is shown for **5** in Fig. 1 [31]. Similarly, the MALP complexes of Sm (**10**) and Y (**11**) are isostructural and crystallize in the triclinic space group $P-1$; a representative structure of this type is shown for **10** in Fig. 2. Selected bond lengths and angles for all five complexes are given in Tables 2 and 3, respectively. The solid state structures of the DALP and MALP complexes are quite similar and are probably best regarded as displaying a distorted octahedral geometry at the metal center with the alkene centroids occupying positions trans to one bridging aryloxide-O (Ct-Ln-$O_{B\text{-}trans}$ angle range: 160.07–166.16°, Table 3). However, this geometry is obviously highly distorted as the angle between the terminal aryloxide-O atoms deviates greatly from 180° (range: 134.82(8)–137.49(13)°) and the angle between the terminal and bridging aryloxide-O is far wider than 90° (range: 101.34(12)–112.36(11)°). The distortion may be viewed as from octahedral towards tetrahedral with the alkene ligands being forced out of the inner coordination sphere. That being said, the distance between the alkenyl carbons of one allyl group of each terminal aryloxide and the metal center (Ln–C_{term} range: 2.928(5)–3.140(4) Å; Ln–C_{int} range: 3.123(3)–3.288(4) Å, Table 2) are far shorter than the sum of the Ln and carbon van der Waals radii in all five structures (van der Waals Ln···C distances range from 3.6 to 3.7 Å for Y to La, assuming r_{VDW} for C is 1.5 Å) [32]. The carbon atoms of the other allyl group on the terminal aryloxide of the DALP complexes (**5**, **6** and **8**) are not within the sum of van der Waals radii and the same is true of all allyl group carbons on the bridging aryloxides in both the DALP and MALP structures. The lanthanide 2,6-diisopropylphenoxide ate complexes, $[La(OAr)_2(THF)(\mu\text{-}OAr)_2]^-[M(THF)n]^+$ ($M = Li$, $n = 1$; $M = Na$, $n = 2$) and $[Ln(OAr)_4]^-M^+$ ($Ln = Nd$, $M = K$; $Ln = La$, $M = Cs$), are interesting in this regard because the saturated isopropyl group is similar to an allyl group yet in this case, the distance from the lanthanide ion to all three isopropyl carbons lies well outside the sum of the van der Waals radii (Ln···C distance > 3.65 Å in all cases and usually >4 Å) [33,34]. Interestingly, these *ate* complexes do feature π-interactions but these are between the arene rings and the alkali metal cations not the lanthanide ions.

The interaction between the allyl alkene carbons and the metal is distinctly asymmetric with the terminal $=CH_2$ group approaching the metal center more closely than the internal CH= group by, on average, 0.12 Å (range: 0.029–0.232 Å, Table 2). It is interesting to note that in all five structures the coordinated alkene C=C

Table 2
Selected bond lengths and bond length differences (Å) for complexes **5**, **6**, **8**, **10** and **11**.[a]

	5 (Nd)	**6** (Er)	**8** (Y)	**10** (Sm)	**11** (Y)
Ln–C_{term}[b]	3.122(6)	3.122(6)	3.128(5)	3.120(4)	3.090(3)
Bound alkene	3.024(5)	2.928(5)	2.970(5)	3.099(3)	3.140(4)
Ln–C_{int}[c]	3.185(6)	3.186(6)	3.187(5)	3.149(4)	3.123(3)
Bound alkene	3.256(5)	3.126(5)	3.153(5)	3.252(3)	3.288(4)
Difference	−0.063	−0.060	−0.059	−0.029	−0.033
Δ = (Ln–C_{term})	−0.232	−0.198	−0.183	−0.153	−0.148
− (Ln–C_{int})					
Coordinated C=C	1.311(2)	1.314(7)	1.323(2)	1.279(5)	1.296(5)
	1.331(7)	1.314(7)	1.310(6)	1.294(5)	1.297(5)
Free C=C	1.274(2)	1.275(4)	1.263(2)	1.267(7)	1.272(7)
Terminal-OAr	1.294(2)	1.272(2)	1.289(2)		
Free C=C	1.300(2)	1.295(2)	1.293(2)	1.271(10)	1.287(11)
Bridging OAr	1.262(8)	1.255(8)	1.256(2)		
Ln-OAr	2.147(3)	2.065(3)	2.064(3)	2.121(2)	2.066(2)
Terminal-OAr	2.160(3)	2.076(3)	2.075(3)	2.135(2)	2.074(2)
Ln-μ-OAr	2.345(3)	2.244(3)	2.273(3)	2.319(2)	2.260(2)
Ln-μ-O′Ar	2.371(3)	2.256(3)	2.254(3)	2.319(2)	2.248(2)
Bridge asymmetry	0.026	0.012	0.019	0.0	0.012
|(Ln-OAr)					
− (Ln-O′Ar)|					

[a] Complete tables of bond lengths including specific labels can be found in the Supplementary Material.
[b] C_{term} refers to the terminal $=CH_2$ carbon of the allyl chain.
[c] C_{int} refers to the internal CH= carbon of the allyl chain.

Table 3
Bond angles around Ln (deg) for complexes **5**, **6**, **8**, **10** and **11**.[a]

	5 (Nd)	**6** (Er)	**8** (Y)	**10** (Sm)	**11** (Y)
O_{T1}-Ln-O_{T2}[b]	135.77(3)	137.49(13)	136.51(12)	134.82(8)	135.51(9)
O_{T1}-Ln-O_B	103.64(11)	101.34(12)	112.36(11)	108.27(7)	107.57(8)
O_{T1}-Ln-O_B'	111.00(11)	111.32(12)	101.68(11)	105.99(7)	110.57(8)
O_{T2}-Ln-O_B	110.10(11)	110.20(11)	104.89(11)	107.55(8)	109.19(7)
O_{T2}-Ln-O_B'	106.87(11)	104.53(12)	110.63(11)	111.31(6)	105.60(7)
O_B-Ln-O_B'	70.19(10)	72.45(13)	72.44(12)	70.48(7)	72.01(7)
Ct1-Ln-Ct2[c]	106.73	105.25	105.57	103.08	101.89
Ct1-Ln-O_{T1}	73.35	74.00	73.69	73.55	70.70
Ct1-Ln-O_{T2}	77.22	76.22	76.14	78.45	82.15
Ct1-Ln-O_B	92.79	93.62	93.28	95.26	91.95
Ct1-Ln-O_B'	162.94	165.55	165.13	165.67	163.67
Ct2-Ln-O_{T1}	86.17	85.12	84.88	89.69	77.27
Ct2-Ln-O_{T2}	71.57	74.23	73.88	82.92	73.44
Ct2-Ln-O_B	160.07	161.10	161.21	161.31	166.16
Ct2-Ln-O_B'	90.17	88.66	90.55	91.23	94.15
Ln-O_B-Ln′	108.81(10)	107.55(13)	107.56(12)	109.56(12)	107.99(7)

[a] Complete tables of bond angles including specific labels can be found in the Supplementary Material.
[b] O_{T1} and O_{T2} refer to the terminal aryloxide-O; O_B and O_B' refer to the symmetry-related bridging aryloxide-O pair.
[c] Ct1 and Ct2 refer to the centroids (midpoints) of the two unique bound alkene carbons.

distance is slightly longer than the non-coordinated alkene units, whether part of the bridging or terminal aryloxide ligand, in the same molecule (Table 2). The difference in coordinated and free alkene bond lengths is much more pronounced in the case of the DALP complexes compared with those containing the MALP ligand. It is not obvious why this should be the case and the fact that there is some disorder in the free allyl groups of some structures suggests that these differences should be viewed with caution.

The aryloxide bonding is largely unexceptional. As expected, the Ln–O bonds for the terminal aryloxide are about 0.2 Å shorter than the bridging aryloxide Ln–O bonds (Table 2). The aryloxides bridge the two lanthanide centers in a symmetrical fashion (asymmetry range: 0.00–0.026 Å). Both the bridging and terminal Ln–O bond distances are somewhat shorter than the distances normally observed in 6-coordinate lanthanide aryloxide dimers. For example, when all distances are corrected to an equivalent 6-coordinate Y^{3+} radius of 0.90 Å [35], the terminal and bridging Ln–O distances in the DALP and MALP complexes fall in the ranges 2.063–2.086 and 2.248–2.288 Å, respectively, while the literature complexes span the ranges 2.103–2.138 and 2.272–2.426 Å for bridging and terminal Ln–O distances [36–40]. The only complexes with comparably short distances are $[Yb(ONaph)_2(THF)(NCCH_3)]_2[\mu\text{-}ONaph]_2$ (ONaph = 1-naphthoxide) and $[Ln(O\text{-}2,6\text{-}C_6H_3(CH_2Ph)_2)_2]_2[\mu\text{-}O\text{-}2,6\text{-}C_6H_3(CH_2Ph)_2]_2$ (Ln = La, Yb) [41,42]. In the former complex, the shorter Ln–O distance is explained by the smaller CH_3CN ligand. However, the latter pair of complexes possess secondary π-arene interactions between one of the bridging aryloxide benyzl groups and the lanthanide centers (η^6-arene in the case of La and both η^3 and η^2 in the case of Yb) [42]. As observed in this work, these π interactions are weak and the bonds long, resulting in less steric crowding at the lanthanide ion and a closer approach of the aryloxide ligands.

There are very few structurally characterized lanthanide–alkene complexes with which to compare the complexes reported here. The majority of these involve divalent lanthanide complexes containing Cp ligands with pendant alkene groups (**I** and **II**) [22,23], although there is one example of an alkyl complex with a coordinated tethered alkene (**IV**, Chart 1) [25]. A series of alkaline earth alkene complexes (**III**) that are closely related to the divalent lanthanide derivatives **II** have also been reported (Chart 1) [24]. The bridging ethylene derivative $(C_5Me_5)_2Yb(\mu\text{-}C_2H_4)Pt(PPh_3)_2$ was reported several years ago but since backbonding from Pt clearly dominates the structural parameters, this complex is not comparable to those reported here [21]. There are also two reports of lanthanide 1,4-diphenylbutadiene complexes but in both cases, the diene ligand is clearly reduced and cannot be compared with the neutral alkene complexes discussed here [43,44]. The only trivalent lanthanide–alkene complex that has been structurally characterized is the $[(C_5Me_4SiMe_2CH_2CH{=}CH_2)_2Sm]^+$ cation of **Id** (Chart 1) [22]. All of these complexes, with the exception of **IV**, also show shorter terminal vs. internal Ln–C distances by *ca.* 0.2 Å on average compared with an average value of 0.12 Å here. In contrast, the alkyl–alkene complex **IV** shows a significantly closer internal vs. terminal Yb–C distance ($\Delta = (Yb{-}C_{term}) - (Yb{-}C_{int}) = +0.30$ Å). Given the very different type of tethering group, it seems likely that whether the internal or terminal carbon approaches the metal most closely is a function of the nature of the tether rather than any intrinsic preference of the metal.

The terminal Ln–C distances in the DALP and MALP complexes described here differ considerably from those found in complexes **I**, **II** and **IV**. When the metal ionic radii are corrected to that of six-coordinate Y^{3+} according to Shannon [35], the divalent complexes **I** and **II**, and the trivalent cationic complex **Id**, predict $Ln{-}C_{term}$ distances in the range 2.73–2.82 Å [22,23]. In fact, the corrected distances in the aryloxide tethered alkene complexes discussed here range from 2.94 to 3.14 Å, more than 0.2 Å longer. Similarly, the Sr^{2+} and Ba^{2+} complexes (**IIIb**–**c**) predict comparable distances (range: 2.71–2.76 Å) [24]. However, the Ca^{2+} complex (**IIIa**) predicts somewhat longer distances of 2.85–2.95 Å and the Mg^{2+} complex shows no alkene coordination in the solid state at all. These results suggest that steric pressure plays a role and it seems likely that the longer Ln–C distances observed in the MALP and DALP complexes is a reflection of weaker alkene bonding due to increased steric crowding for the smaller trivalent lanthanide ions with a larger aryloxide ligand. It is noteworthy that the Ln–arene π-interactions

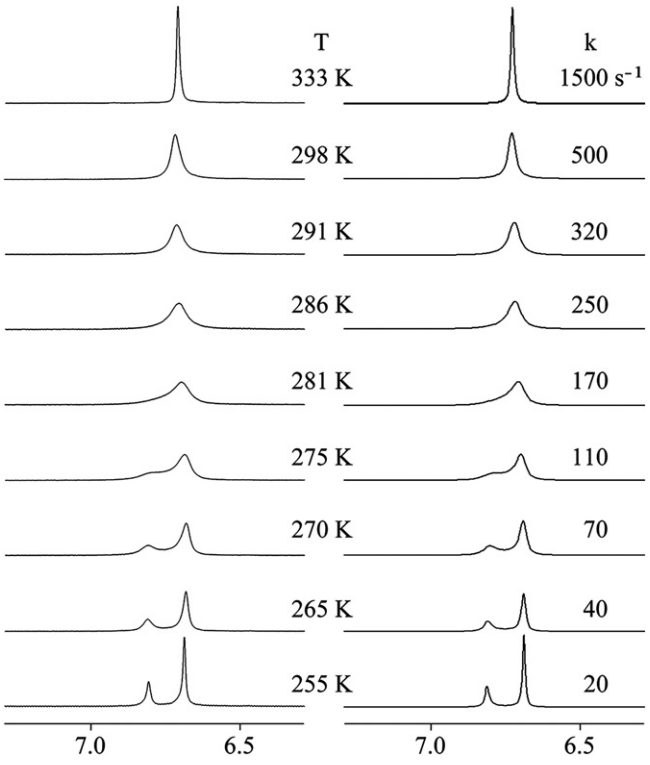

Fig. 3. Observed and simulated ^1H NMR (360 MHz) spectra for the *m*-aryl proton region of $\{Y[DALP]_2\}_2[\mu\text{-}DALP]_2$ (**8**) between 333 and 255 K in d_{14}-methylcyclohexane.

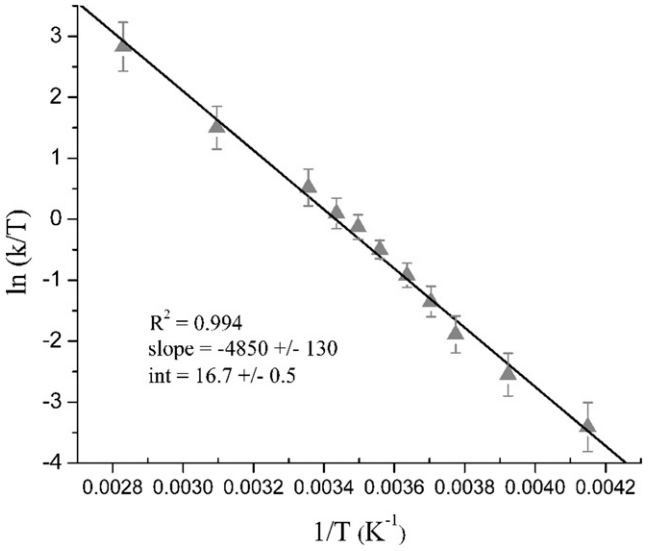

Fig. 4. Eyring plot for the bridge–terminal aryloxide exchange process of $\{Y[DALP]_2\}_2[\mu\text{-}DALP]_2$ (**8**) in d_{14}-methylcyclohexane.

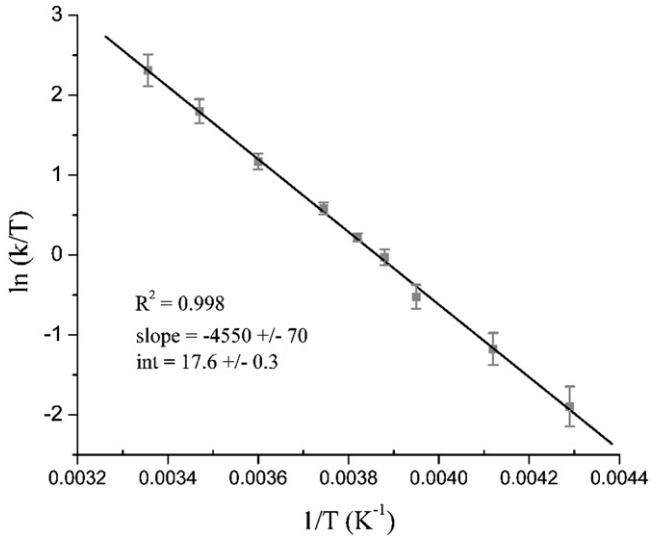

Fig. 5. Eyring plot for the bridge–terminal aryloxide exchange process of {La[DALP]$_2$}$_2$[μ-DALP]$_2$ (**3**) in d_{14}-methylcyclohexane.

observed in [Ln(O-2,6-$C_6H_3(CH_2Ph)_2)_2$]$_2$[μ-O-2,6-$C_6H_3(CH_2Ph)_2$]$_2$ (Ln = La, Yb) give similar Ln-π-arene C distances after correction for differences in radii (estimated range 2.9–3.2 Å) [42].

The median bond C=C bond length in complexes **I**–**IV** is 1.32 Å, very similar to the 1.31 Å found in the present work, but in both the literature structures and those reported here, the coordinated C=C bond length covers a very wide range (1.267(11)–1.361(2) Å [22–25]; Table 2). This variability makes it difficult to state with confidence whether the small increase in average C=C bond length for the coordinated vs. non-coordinated alkenes is real but it is clear that any changes in bond length that do occur on coordination are minor.

3.2. Solution behavior of the diamagnetic complexes

In view of the alkene coordination observed in the solid state, we sought evidence for alkene bonding in solution by NMR spectroscopy. At room temperature, the diamagnetic complexes **3** and **8** show a single set of resonances for the DALP ligands in deuterated benzene, toluene or methylcyclohexane. This suggests either that the complexes exist as monomers or are undergoing rapid bridge–terminal aryloxide exchange. On cooling below room temperature in either d_8-toluene or d_{14}-methylcyclohexane, the ^{1}H NMR resonances of either **3** or **8** broaden and eventually decoalesce into two sets of DALP resonances in 2:1 ratio, clearly indicating that these complexes are dimeric in non-coordinating solvents at room temperature. No concentration effects are observed over at least a five-fold concentration range, consistent with an intact dimer. However, the addition of a small amount of d_8-THF (5:1 d_8-toluene:d_8-THF) results in sharp spectra with a single set of DALP resonances down to at least 200 K, clearly indicating that THF cleaves the dimeric structure into a monomer (Eq (1)).

$$\{Ln(DALP)_2\}_2[\mu\text{-}DALP]_2 \xrightarrow{THF} 2\ Ln(DALP)_3(THF)_n \quad (1)$$

Ln = La (**3**), Ce (**4**), Nd (**5**), Er (**6**), Yb (**7**), Y (**8**)

3.2.1. Dynamic bridge–terminal aryloxide exchange

Bridge–terminal aryloxide exchange was examined in more detail for **8** in d_{14}-methylcyclohexane. The dynamic behavior of the *m*-aryl proton resonance was the most easily followed. Fig. 3 shows the observed and simulated spectra for this resonance between 333 and 255 K [45]. An Eyring plot for this resonance, shown in Fig. 4, yielded $\Delta H^{\ddagger} = 40 \pm 1$ kJ mol^{-1}, $\Delta S^{\ddagger} = -59 \pm 4$ J mol^{-1} K^{-1} and $\Delta G^{\ddagger}_{298} = 58 \pm 3$ kJ mol^{-1}. The Eyring plot for the same process and resonance of **3**, shown in Fig. 5, gave $\Delta H^{\ddagger} = 37.8 \pm 0.6$ kJ mol^{-1}, $\Delta S^{\ddagger} = -51 \pm 3$ J mol^{-1} K^{-1} and $\Delta G^{\ddagger}_{298} = 53 \pm 2$ kJ mol^{-1}. The negative entropy term for bridge–terminal aryloxide exchange is noteworthy since it argues against cleavage of the bridge during exchange. One possible explanation for the negative entropy term is that exchange occurs by way of a crowded, triple aryloxide bridge like that shown in Eq (2). This would no doubt involve alkene dissociation (see evidence for this below) which would make a positive entropy contribution, but the crowding of such an intermediate would likely prevent aryloxide rotation and the increased rigidity would be expected to result in an overall negative entropy term. The marginally lower barrier to bridge–terminal aryloxide exchange for the La complex **3** vs. Y complex **8** could also be taken as evidence for the process shown in Eq (2) given the considerably larger size of La^{3+}.

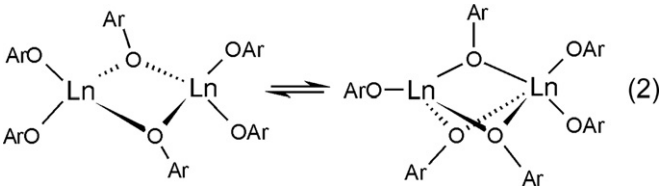

3.2.2. Evidence for weak alkene binding

On further cooling below 255 K, the ^{1}H NMR of **8** in d_{14}-methylclohexane again begins to broaden and the terminal DALP resonances eventually decoalesce just before the solubility limit of the complex at 188 K. While there is significant broadening of all resonances at this temperature due to viscosity effects, the larger *m*-aryl proton resonance observed at 255 K splits into two resonances of equal intensity by 188 K. This is consistent with the solid state structure and indicates that at this temperature alkene exchange is slow. The observed and simulated spectra for this process and the corresponding Eyring plot are shown in Figs. 6 and 7, respectively. Values of $\Delta H^{\ddagger} = 50 \pm 4$ kJ mol^{-1}, $\Delta S^{\ddagger} = +46 \pm 15$ J mol^{-1} K^{-1} and $\Delta G^{\ddagger}_{298} = 36 \pm 15$ kJ mol^{-1} were obtained from Fig. 7. Although these activation parameters are prone to considerable error, the entropy term obtained for this process is so substantially positive that we believe it is significant. If so, it indicates a dissociative alkene exchange process and the barrier observed would represent the sum of the barrier to alkene dissociation and aryloxide rotation.

It might be expected that alkene bonding would be detectable by chemical shift differences between alkene proton or carbon resonances in the complex relative to free alkene by NMR spectroscopy.

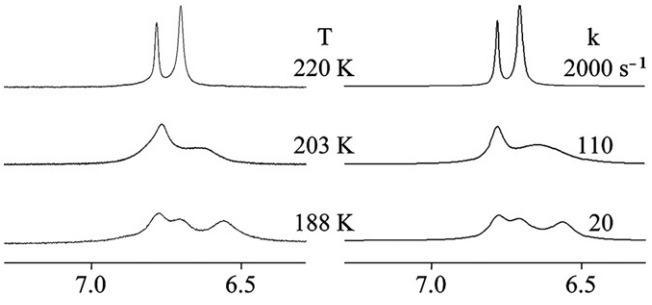

Fig. 6. Observed and simulated ^{1}H NMR (360 MHz) spectra for the *m*-aryl proton region of {Y[DALP]$_2$}$_2$[μ-DALP]$_2$ (**8**) between 255 and 188 K in d_{14}-methylcyclohexane.

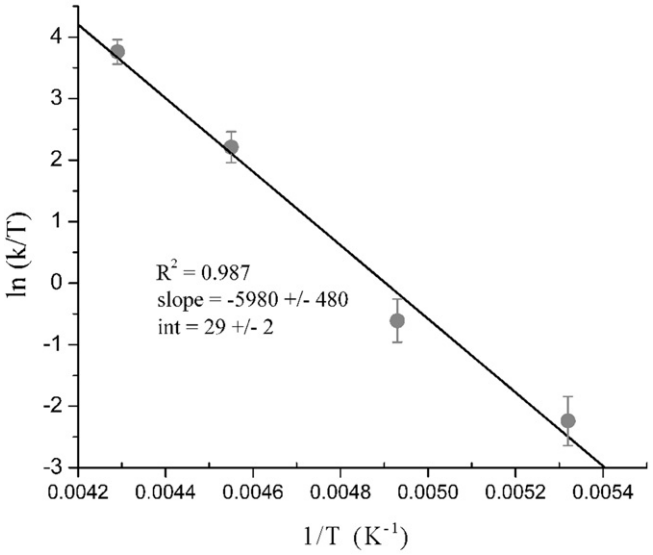

Fig. 7. Eyring plot for the terminal aryloxide alkene exchange process of {Y[DALP]$_2$}$_2$[μ-DALP]$_2$ (**8**) in d_{14}-methylcyclohexane.

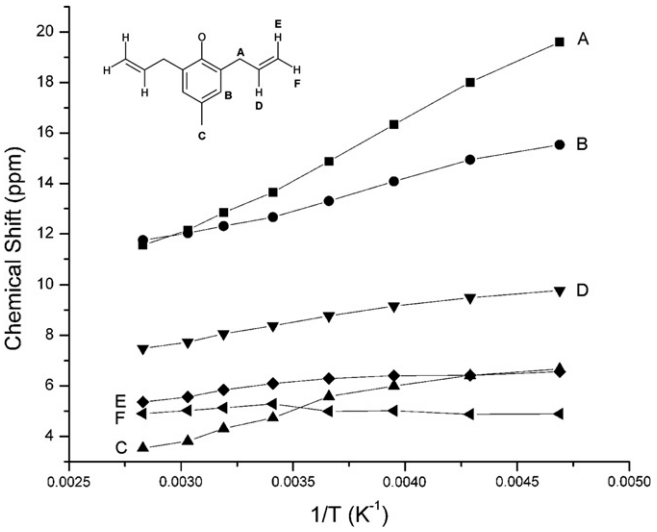

Fig. 9. ^{1}H NMR Chemical shift δ vs. $1/T$ for {Nd[DALP]$_2$}$_2$[μ-DALP]$_2$ (**5**) in 5:1 d_8-toluene:d_8-THF (360 MHz).

Casey et al., for example, have shown that the ^{1}H NMR chemical shift difference, $\Delta\delta$, between the terminal $=CH_2$ protons in $Cp_2Y(\eta^1{:}\eta^2$-$CH_2CH_2CR_2CR'{=}CH_2)$ (R = H, Me; R′ = H, Me) is between about 0.6 and 1.5 ppm in the coordinated alkene complex but <0.1 ppm for either the free alkene equivalent or the complex in the presence of d_8-THF (where alkene displacement by THF is assumed) [12–17]. However, in the diamagnetic complexes **3**, **8**, **9** and **11** at room temperature in d_8-toluene, $\Delta\delta$ is <0.1 ppm. Similarly, other lanthanide–alkene complexes **I**, **II** and the alkaline earth complexes **III** also show $\Delta\delta < 0.1$ ppm in non-coordinating solvents [22–24]. The alkene carbon ^{13}C NMR chemical shifts, however, are more sensitive to alkene coordination with the terminal carbon shifting upfield and the internal carbon downfield by several ppm. For example, the $Cp_2Y(\eta^1{:}\eta^2$-$CH_2CH_2CR_2CR'{=}CH_2)$ (R = H, Me; R′ = H, Me) complexes reported by Casey et al, show an *increase* in the coordinated alkene internal–terminal ^{13}C chemical shift difference of, on average, *ca.* 17 ppm ($\Delta\Delta\delta_c$ range: 13.8–25.0 ppm) relative to the free ligand [12–16]. The divalent Yb complexes **I** and **II** show $\Delta\Delta\delta_c$ values of 9.6 and 18.1 ppm, respectively, while the related alkaline earth complexes **III** have an average $\Delta\Delta\delta_c$ value of 9.7 ppm (range: 8.9–10.9 ppm) [22–24]. At room temperature, the diamagnetic DALP complexes of La (**3**) and Y (**8**) show smaller $\Delta\Delta\delta_c$ values of 2.7 and 2.5 ppm, respectively, while this difference is somewhat larger

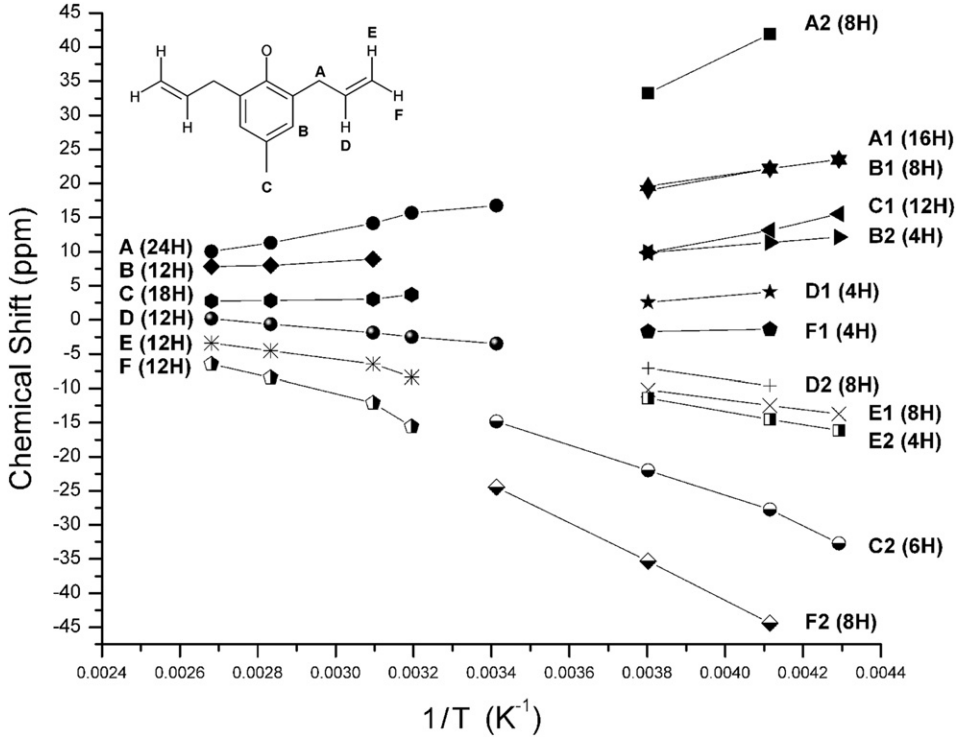

Fig. 8. ^{1}H NMR Chemical shift δ vs. $1/T$ for {Nd[DALP]$_2$}$_2$[μ-DALP]$_2$ (**5**) in d_8-toluene (360 MHz).

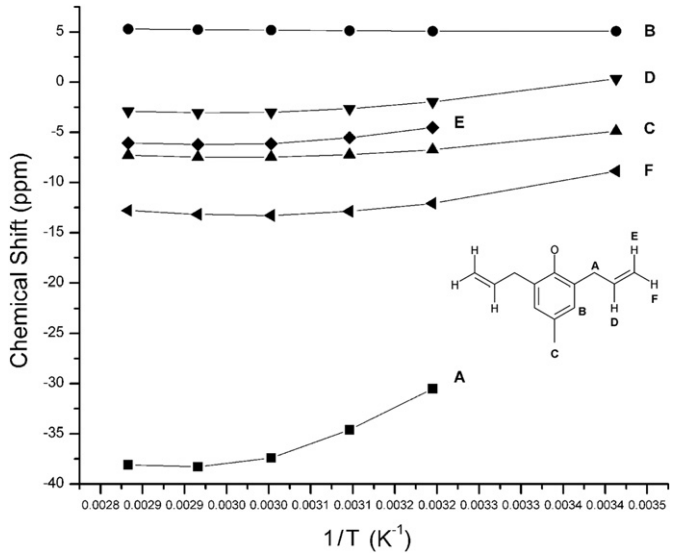

Fig. 10. ^{1}H NMR Chemical shift δ vs. $1/T$ for {Er[DALP]$_2$}$_2$[μ-DALP]$_2$ (**6**) in 5:1 d_8-toluene:d_8-THF (360 MHz).

in the corresponding MALP complexes (**9**, 5.7; **11**, 6.0 ppm). The ^{13}C NMR spectrum of **8** recorded at 203 K shows two distinct sets of resonances in 2:1 ratio for the terminal and bridging aryloxides, respectively. At 203 K, the alkenyl carbon $\Delta\Delta\delta_c$ value for the terminal aryloxide increases by 4.7 ppm while that for the bridging aryloxide *decreases* by −4.6 ppm. At this temperature, alkene exchange is still rapid in the ^{13}C NMR spectrum, so the observed $\Delta\Delta\delta_c$ value is an average of that for free (by definition $\Delta\Delta\delta_c = 0$) and coordinated alkene. In order to properly compare this parameter to that observed in other alkene complexes mentioned above, it therefore must be doubled to 9.4 ppm, a value that is very similar to that observed for **I** and **III** [22,24], but smaller than those observed in the tethered alkyl–alkene complexes [12–16].

3.3. Paramagnetic complexes: variable temperature ^{1}H NMR

The paramagnetic DALP complexes **4** (Ce), **5** (Nd), **6** (Er) and **7** (Yb) were studied by variable temperature ^{1}H NMR in both d_8-toluene and 5:1 d_8-toluene:d_8-THF between about 210 and 380 K. Plots of δ vs. $1/T$ in d_8-toluene and 5:1 d_8-toluene:d_8-THF are shown for $Nd_2(DALP)_6$ (**5**) in Figs. 8 and 9, respectively; complete tables of NMR chemical shifts including line widths at half height and δ vs. $1/T$ plots are given for **4**, **6** and **7** in the Supplementary Material. In the case of **5**, decoalescence for bridge–terminal aryloxide exchange occurs between *ca.* 275 and 295 K, depending on the separation of the resonances involved (Fig. 8). There is no evidence for decoalescence due to the alkene exchange process at lower temperatures but the extremely broad line widths, in some cases >2000 Hz, below about 250 K make it impossible to discern the onset of this second process. Addition of d_8-THF simplifies the spectra to 6 resonances and completely alters the variable temperature behavior (Fig. 9). The resonances in Fig. 9 follow fairly linear δ vs. $1/T$ behavior consistent with formation of a monomeric $Nd(DALP)_3(THF)_n$ complex at all temperatures. The behavior of Ce complex **4** is very similar to **5** with approximately the same decoalescence temperature for bridge–terminal aryloxide exchange. The variable temperature ^{1}H NMR behavior of $Yb_2(DALP)_6$ (**7**) was only examined at room temperature and above (297–377 K) but a maximum of 6 resonances was observed indicating that this complex too is in the fast bridge–terminal aryloxide exchange region in this temperature range.

In contrast to **4** and **5**, $Er_2(DALP)_6$ (**6**) shows evidence for up to 12 distinct resonances throughout the temperature range studied (253–357 K) indicating that bridge–terminal aryloxide exchange remains slow on the NMR timescale. This is a reflection of the large pseudo-contact shifts observed for Er^{3+} as evident from the total chemical shift range of >250 ppm at 298 K. In the presence of d_8-THF, the spectra again simplify to only 6 resonances indicating formation of a monomeric THF adduct, $Er(DALP)_3(THF)_n$ (Fig. 10). Interestingly, the resonances of this THF adduct show distinct curvature between 293 and 353 K. This may be due to an equilibrium between species with different numbers of coordinated THF molecules, Eq (3).

$$Er(DALP)_3(THF)_n \underset{THF}{\overset{-THF}{\rightleftharpoons}} Er(DALP)_3(THF)_{n-1} \qquad (3)$$

4. Conclusions

The *ortho*-allyl substituted aryloxide ligands DALP and MALP form dimeric complexes with trivalent lanthanides and yttrium that contain weak Ln–alkene bonds in the solid state with allyl groups on the terminal aryloxides. The Ln–alkene structural parameters indicate, in common with the small number of reported lanthanide and alkaline earth alkene complexes, that the terminal alkene carbon approaches the metal more closely than the internal alkene carbon. However, bond length comparisons clearly indicate that the Ln–C distances observed in our work are significantly longer than those reported in **I**–**IV** after correction for differences in ionic radii.

The dimeric complexes undergo bridge–terminal aryloxide exchange at room temperature in solution for all complexes except that of Er. In the case of the diamagnetic complex $Y_2(DALP)_6$, a second dynamic process consistent with alkene exchange was observed at very low temperature. This fact, coupled with the observation of a significant increase in the chemical shift difference between the terminal and internal alkene carbons relative to free alkene for the terminal but not bridging aryloxide ligands, strongly suggests that the Ln–alkene interaction persists in non-coordinating solvent such as toluene or methylcyclohexane. In contrast, the complex is completely cleaved to a monomer in the presence of THF and shows no evidence for alkene coordination in this solvent as might be expected.

Acknowledgment

The support of the Natural Sciences and Engineering Research Council of Canada is gratefully acknowledged.

Appendix A. Supplementary material

Part 1: Tables of atomic coordinates, bond distances and angles and anisotropic thermal parameters for **5**, **6**, **8**, **10** and **11**.

Part 2: Variable temperature ^{1}H NMR data for paramagnetic complexes **4**–**7** in d_8-toluene and d_8-toluene:d_8-THF (5:1).

Supplementary data associated with this article can be found, in the online version, at doi:10.1016/j.jorganchem.2010.09.004.

References

[1] F.T. Edelmann, Chem. Soc. Rev. 38 (2009) 2253–2268.
[2] B. Corneils, W.A. Hermann (Eds.), Applied Homogeneous Catalysis with Organometallic Compounds, Wiley-VCH, Weinheim, Germany, 1996.
[3] F.T. Edelmann, Coord. Chem. Rev. 253 (2009) 343–409.
[4] W. Chen, F. Wang, Sci. China, Ser. B: Chem. 52 (2009) 1520–1543.

[5] L. Porri, G. Ricci, A. Giarusso, N. Shubin, Z. Lu, Recent developments in lanthanide catalysts for 1,3-diene polymerization. in: P. Arjunan, J.E. McGrath, T.L. Hanlon (Eds.), Olefin Polymerization: Emerging Frontiers, ACS Symposium Series, vol. 749, 1999, pp. 15–30.
[6] W.J. Evans, D.G. Giarikos, J.W. Ziller, Organometallics 20 (2001) 5751–5758.
[7] H.F. Yuen, T.J. Marks, Organometallics 27 (2008) 155–158 and references therein.
[8] G. Zi, L. Xiang, H. Song, Organometallics 27 (2008) 1242–1246.
[9] D.V. Vitanova, F. Hampel, K.C. Hultzsch, J. Organomet. Chem. 69 (2007) 4690–4701.
[10] S. Hong, T.J. Marks, Acc. Chem. Res. 37 (2004) 673–686.
[11] S.P. Nolan, T.J. Marks, J. Am. Chem. Soc. 111 (1989) 8538–8542.
[12] C.P. Casey, S.L. Hallenback, D.W. Pollock, C.L. Landis, J. Am. Chem. Soc. 117 (1995) 9770–9771.
[13] C.P. Casey, S.L. Hallenback, J.M. Wright, C.L. Landis, J. Am. Chem. Soc. 119 (1997) 9680–9690.
[14] C.P. Casey, M.A. Fagan, S.L. Hallenback, Organometallics 17 (1998) 287–289.
[15] C.P. Casey, J.J. Fisher, Inorg. Chim. Acta 270 (1998) 5–7.
[16] C.P. Casey, J. Fisher Klein, M.A. Fagan, J. Am. Chem. Soc. 122 (2000) 4320–4330.
[17] C.P. Casey, T.Y. Lee, J.A. Tunge, D.W. Carpenetti II, J. Am. Chem. Soc. 123 (2001) 10762–10763.
[18] C.P. Casey, J.A. Tunge, T.Y. Lee, D.W. Carpenetti II, Organometallics 21 (2002) 389–396.
[19] C.P. Casey, J.A. Tonge, M.A. Fagan, J. Organomet. Chem. 663 (2002) 91–97.
[20] C.P. Casey, J.A. Tunge, T.Y. Lee, M.A. Fagan, J. Am. Chem. Soc. 125 (2003) 2641–2651.
[21] C.J. Burns, R.A. Andersen, J. Am. Chem. Soc. 109 (1987) 915–917.
[22] W.J. Evans, J.M. Perotti, J.C. Brady, J.W. Ziller, J. Am. Chem. Soc. 125 (2003) 5204–5212.
[23] H. Schumann, A. Heim, S. Schutte, D. Lentz, Z. Anorg. Allg. Chem. 632 (2006) 1939–1942.
[24] H. Schumann, S. Schutte, H.J. Kroth, D. Lentz, Angew. Chem. Int. Ed. Engl. 43 (2004) 6208–6211.
[25] C. Eaborn, P.B. Hitchcock, K. Izod, Z.R. Lu, J.D. Smith, Organometallics 15 (1996) 4783–4790.
[26] D.C. Bradley, J.S. Ghotra, F.A. Hart, J. Chem. Soc., Dalton Trans. (1973) 1021–1023.
[27] G.M. Sheldrick, SHELXTL: v6.10, Structure Determination Software Suite [Computer Program]. Bruker AXS, Madison, WI, 2001.
[28] G.M. Sheldrick, SADABS: v2.01, Empirical Absorption Correction Program [Computer Program]. Bruker AXS, Madison, WI, 2001.
[29] G.M. Sheldrick, SHELXS97: Structure Solution Software [Computer Program]. Bruker AXS, Madison, WI, 1997.
[30] I.S. Orlov, A.A. Moiseeva, K.P. Butin, M.P. Egorov, Russ. Chem. Bull., Int. Ed. 51 (2002) 1961–1962.
[31] L.J. Ferrugia, J. Appl. Cryst. 30 (1997) 565–566.
[32] S.-Z. Hu, Z.-H. Zhou, B.E. Robertson, Z. Kristallogr. 224 (2009) 375–383.
[33] D.L. Clark, J.G. Watkin, J.C. Huffman, Inorg. Chem. 31 (1992) 1554–1556.
[34] D.L. Clark, R.V. Hollis, B.L. Scott, J.G. Watkin, Inorg. Chem. 35 (1996) 667–674.
[35] R.D. Shannon, Acta Cryst. A 32 (1976) 751–767.
[36] T.J. Boyle, L.J. Tribby, S.D. Bungey, Eur. J. Inorg. Chem. (2006) 4553–4563.
[37] G.B. Deacon, C.M. Forsyth, R. Harika, P.C. Junk, J.W. Ziller, W.J. Evans, J. Mater. Chem. 14 (2004) 3144–3149.
[38] W.J. Evans, J.M. Olofson, J.W. Ziller, Inorg. Chem. 28 (1989) 4308–4309.
[39] G.R. Giesbrecht, J.C. Gordon, D.L. Clark, B.L. Scott, J.G. Watkin, K.J. Young, Inorg. Chem. 41 (2002) 6372–6379.
[40] W.J. Evans, M.A. Ansari, S.I. Khan, Organometallics 14 (1995) 558–560.
[41] J. Carretas, J. Branco, J. Marcalo, P. Isolani, A. Domingos, A.P. de Matos, J. Alloys Compd. 323 (2001) 169–172.
[42] M.L. Cole, G.B. Deacon, P.C. Junk, K.M. Proctor, J.L. Scott, C.R. Strauss, Eur. J. Inorg. Chem. (2005) 4138–4144.
[43] K. Mashima, H. Sugiyama, A. Nakamura, J. Chem. Soc., Chem. Commun. (1994) 1581–1582.
[44] N.S. Emelyanova, A.A. Trifonov, L.N. Zakharov, A.F. Shestakov, Y.T. Struchkov, M.N. Bochkarev, J. Organomet. Chem. 540 (1997) 1–6.
[45] H.J. Reich, WINDNMR, Vers. 7.1.13 [Computer Program], Madison, WI, 2008.